

# In situ characterization of qubit control lines: a qubit as a vector network analyzer

Markus Jerger,<sup>1</sup> Zénon Vasselin,<sup>1</sup> and Arkady Fedorov<sup>1,2,\*</sup>

<sup>1</sup>*ARC Centre of Excellence for Engineered Quantum Systems,  
The University of Queensland, St Lucia QLD 4072, Australia*

<sup>2</sup>*School of Mathematics and Physics, University of Queensland, Brisbane, Queensland 4072, Australia*  
(Dated: October 17, 2022)

We present a technique to measure the transfer function of a control line using a qubit as a vector network analyzer. Our method requires coupling the line under test to the longitudinal component of the Hamiltonian of the qubit and the ability to induce Rabi oscillations through simultaneous driving of the transversal component. We used this technique to characterize the 'flux' control of a superconducting Transmon qubit in the range of 8 to 400 MHz. Our method can be used for the qubit 'flux' line calibration to increase the fidelity of entangling gates for the quantum processor. The qubit can be also used as a microscopic probe of the electro-magnetic fields on a chip.

Characterization of the transfer function of a microwave line from the room temperature electronics down to a chip at low temperatures has important applications. In quantum control and computing it allows for corrections of distortions of a control signal and can be used to increase the fidelity of quantum operations. In particular, the gates which involve non-adiabatic frequency tuning of quantum bits are extremely sensitive to these distortions and require precise calibration [1–5]. The most common approach to deal with this problem is to measure the transfer function at room temperature using a vector network analyzer for frequency domain measurements or an oscilloscope for time-domain characterization (see, for example, Ref. [5]).

This method has two important deficiencies: the transfer function of the line changes when the setup is cooled to cryogenic temperatures and the part of the signal line from the microwave connector closest to the chip to the qubit is not included in the characterization. Various methods for *in situ* line calibration have been proposed. Some calibrations are limited in time resolution by the length of the microwave  $\pi$ -pulse [1, 3, 5], others are applicable only to specific systems [2] or pulses [6], and most procedures typically provide only indirect information about the transfer function. In this Letter we propose a method of *in situ* direct reconstruction of the response of a control line of a qubit in a large frequency range using the qubit itself.

To understand the principles underlying our method consider the Hamiltonian of a qubit with time dependent longitudinal (frequency control) and transversal (excitation) drives

$$H = \frac{\hbar}{2}\omega_0\sigma_z + \hbar A_x \cos(\omega_x t + \phi_x)\sigma_x + \hbar A_z \cos(\omega_z t + \phi_z)\sigma_z. \quad (1)$$

After transformation into the rotating frame with  $U_1 = e^{-i(\omega_x t + \phi_x)\sigma_x/2}$ , the Hamiltonian reads

$$H' = \frac{\hbar}{2}A_x\sigma'_x + \frac{\hbar}{2}\delta\omega\sigma'_z + \hbar A_z \cos(\omega_z t + \phi_z)\sigma'_z, \quad (2)$$

where  $\delta\omega = \omega_0 - \omega_x$  is the detuning of the excitation driving and we have used the rotating wave approximation under the assumption  $A_x \ll \omega_0$ . Note that the transversal phase does not explicitly appear in the Hamiltonian (2), however it implicitly provides a reference for the rotating frame through the transformation operator. The time-independent part of  $H'$  can be diagonalized with  $U_2 = e^{-i\phi_t\sigma'_y}$ ,  $\phi_t = -\arctan(\delta\omega/A_x)$ , as

$$\tilde{H}' = \frac{\hbar}{2}\Omega_R\tilde{\sigma}'_x + \frac{\hbar}{2}\omega_R \cos(\omega_z t + \phi_z)\tilde{\sigma}'_z, \quad (3)$$

where  $\Omega_R = \sqrt{A_x^2 + \delta\omega^2}$  is the Rabi frequency and  $\omega_R = A_x A_z / \Omega_R$ . In the special case of  $\delta\omega = 0$ ,  $U_2$  reduces to the identity,  $\Omega_R = A_x$  and  $\omega_R = A_z$ .

Comparing (1) and (3), we observe that in the rotating frame the  $z$  term plays the role of a transversal drive for the dressed-state qubit with splitting  $\Omega_R$  and will induce Rabi oscillations with frequency  $\omega_R$ . To make this observation explicit we transform the Hamiltonian (3) into the second rotating frame for  $\omega_z = \omega_R$  with  $U_3 = e^{-i(\omega_z t)\tilde{\sigma}'_x/2}$  to obtain

$$H'' = \frac{\hbar}{2}\omega_R (-\sin\phi_z\sigma''_y + \cos\phi_z\sigma''_z), \quad (4)$$

where we have used another rotating wave approximation with  $\omega_R \ll \Omega_R$ . The Hamiltonian  $H''$  shows that the amplitude  $A_z$  and phase  $\phi_z$  of the  $z$  control are encoded in the frequency and axis of the Rabi oscillations of the dressed-state qubit and can be measured in the experiment.

By setting  $\delta\omega = 0$  and varying  $A_x$  one can perform the experiment for different  $\omega_z$  and identify the transfer function of the  $z$  line in the range of frequencies  $\Gamma_1, \Gamma_2 \ll \omega_z \ll \omega_0$  which are most relevant for the frequency control of the qubit with  $\Gamma_{1,2}$  being the relaxation and dephasing rates of the qubit, respectively.

For weakly anharmonic qubits, such as the transmon, the two-level approximation becomes invalid when the Rabi frequency approaches the anharmonicity,  $\sim 300$  MHz. To overcome this problem we can exploit

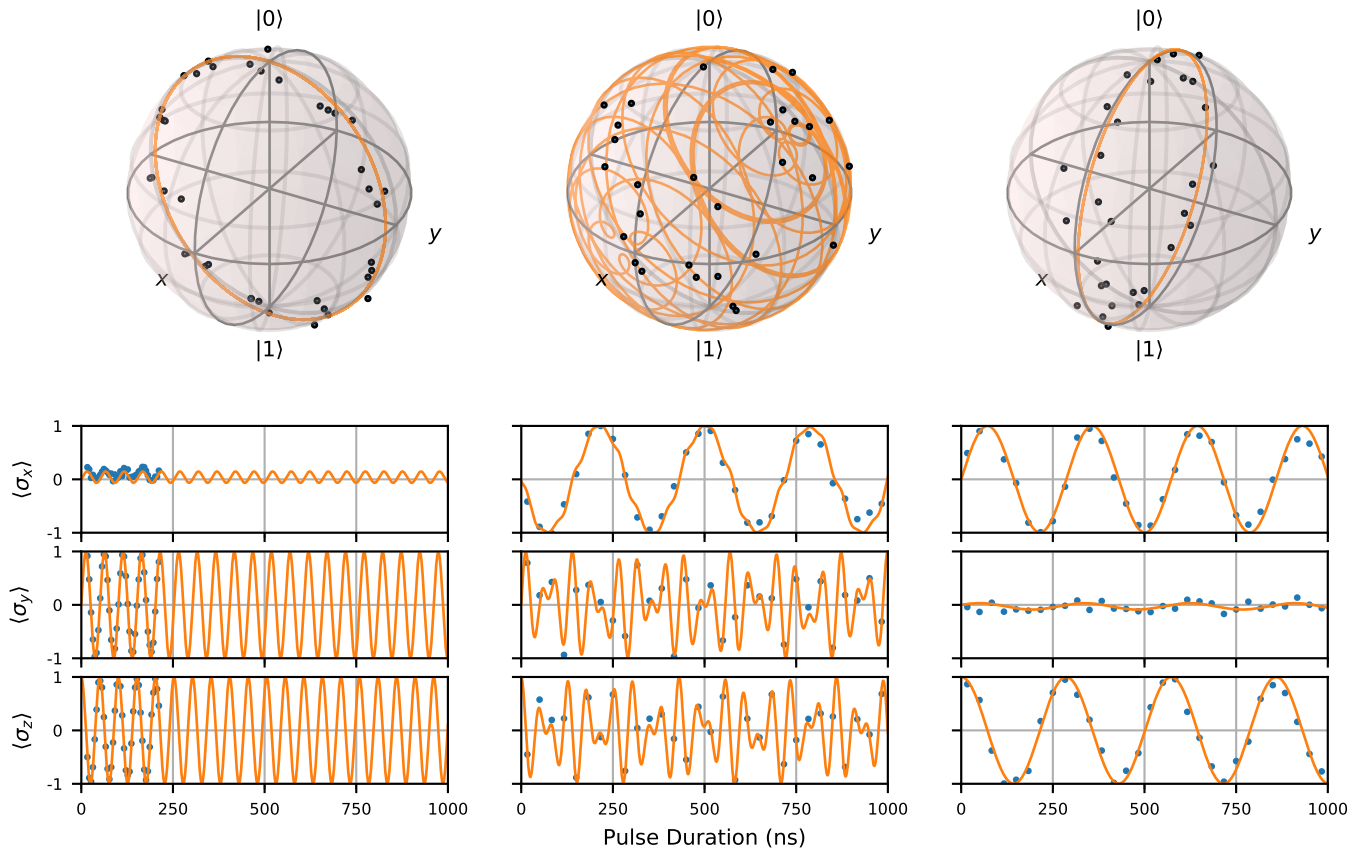


FIG. 1. A typical data set for  $\Omega_R = 19.8$  MHz and the corresponding trajectories of the Bloch vector in the first and second rotating frames. a) State tomography of the qubit with only the  $x$  drive applied. The fit yields a rotation vector of  $\vec{\Theta}=(19.7,-1.9,0.8)$  MHz and  $\phi_x = -0.1$ . b) State tomography of the qubit with both the  $x$  and  $z$  drives applied. The frequency of  $z$  drive is set to  $\omega_z = \Omega_R$ . The sampling rate of the experiment is chosen such that the slow oscillations at  $\omega_R$  can be resolved unambiguously but not necessarily the fast oscillations at  $\Omega_R$ , which are cancelled by  $U_3$ . The orange curve shows the theoretical dynamics derived from the fit in (c). c) The dynamics of the qubit in the second rotating frame, transformed from (b). The fit yields  $\vec{\theta}=(0.2,-3.5,0.1)$  MHz and we can obtain  $A_z = 3.5$  MHz and  $\phi_z = 1.54$ .

off-resonant driving ( $\delta\omega \neq 0$ ). In this case we can extend the analysis to higher frequencies at the expense of the signal amplitude.

Both  $A_z$  and phase  $\phi_z$  for a given frequency  $\omega_z$  can be determined directly from the observables in the laboratory or the first rotating frames, such as the excited state population of the qubit. However, it is more convenient to perform tomography and reconstruct the oscillation of the qubit state in the second rotating frame by post-processing. Removing the fast population oscillation with frequency  $\omega_0$ ,  $\Omega_R$  and leaving only the signal varying with the frequency  $\omega_R$  allows for a substantial reduction of the required sampling rate and more robust fitting. The experimental procedure is summarized by the following steps.

- Apply  $x$ -drive with  $z$ -drive off ( $A_z = 0$ ) and fit data to extract  $\Omega_R$  (Fig. 1a).

- Set  $\omega_z = \Omega_R$  and use tomography pulses to reconstruct  $\langle \sigma'_x(t) \rangle$ ,  $\langle \sigma'_y(t) \rangle$  and  $\langle \sigma'_z(t) \rangle$  in the first rotating frame (Fig. 1b).
- Post-process the data to reconstruct  $\langle \sigma''_x(t) \rangle$ ,  $\langle \sigma''_y(t) \rangle$  and  $\langle \sigma''_z(t) \rangle$  in the second rotating frame (Fig. 1c).
- Fit the resulting data to Rabi oscillations described by (4) to extract  $A_z$  and  $\phi_z$  for given  $\omega_z$ .
- Repeat the sequence for different  $\Omega_R$  to cover the necessary frequency range.

In the following we describe the experimental steps in more detail and directions for efficient implementation of the procedure. We tested our method on a standard circuit quantum electrodynamics system: a transmon qubit coupled to a readout resonator with local charge and flux

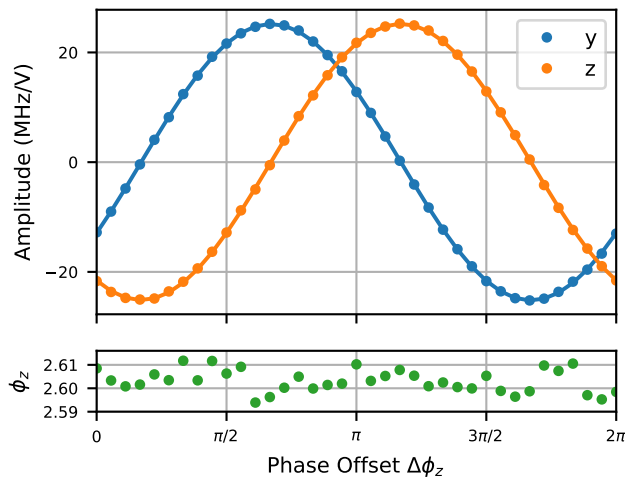


FIG. 2. *Quality of the phase reconstruction* – (top) Measured  $y$  and  $z$  components of the Rotation vector of the dressed qubit as the phase of the longitudinal driving pulse programmed at the AWG is varied. (bottom) Phase  $\phi_z$  of the system function of the control line extracted from the above.

lines. More specifically, we choose the QB 2 of a chip virtually identical to one used in Ref. [7].

*Step 0:* Make sure (1) is a good approximation of the physical system. In case of the transmon and other superconducting qubits, that means choosing a magnetic flux bias and offset (longitudinal driving) amplitude that result in a predominantly linear dependence of the qubit transition frequency on the offset.

*Step 1:* Apply an  $x$  drive to the qubit with the  $z$  drive off. The  $x$  drive can use square pulses or any pulse shape with an envelopes that has a constant amplitude section. Sweep the duration of the constant amplitude section to observe Rabi oscillations. Perform tomography to reconstruct the evolution of a state vector  $\vec{v}(t) = (\langle\sigma_x(t)\rangle, \langle\sigma_y(t)\rangle, \langle\sigma_z(t)\rangle)$  in the first rotating frame (see Fig. 1a).

Fit  $\exp(\vec{\Theta}_{Rt} \cdot \vec{L})\vec{v}(0)$  to this data with fitting parameters  $\vec{\Theta}_R = (\Theta_x, \Theta_y, \Theta_z)$ . Here,  $t$  is the duration of the constant amplitude section of the pulses and  $\vec{L} = (L_x, L_y, L_z)$ ,  $L_x = \begin{pmatrix} 0 & 0 & 0 \\ 0 & 0 & -1 \\ 0 & 1 & 0 \end{pmatrix}$ ,  $L_y = \begin{pmatrix} 0 & 0 & 1 \\ 0 & 0 & 0 \\ -1 & 0 & 0 \end{pmatrix}$ ,  $L_z = \begin{pmatrix} 0 & -1 & 0 \\ 1 & 0 & 0 \\ 0 & 0 & 0 \end{pmatrix}$  are the SO(3) generators of rotations about the  $x$ ,  $y$  and  $z$  axis, respectively, and  $\vec{v}(0) = (0, 0, -1)$  is the initial state of the system. The direction of  $\vec{\Theta}$  determines the axis of rotation of the state vector on the Bloch sphere and the absolute value gives the Rabi frequency  $|\vec{\Theta}| = \Omega_R$ . If non-square pulses are used,  $\vec{v}(0)$  can be made a fitting parameter to absorb the attack of the pulses.

Ideally we expect  $\vec{\Theta} = (A_x, 0, \delta\omega)$ . However in the experiment we often observed small spontaneous detuning of the qubit  $\Theta_z \neq 0$  at larger amplitudes  $A_x$ . As an

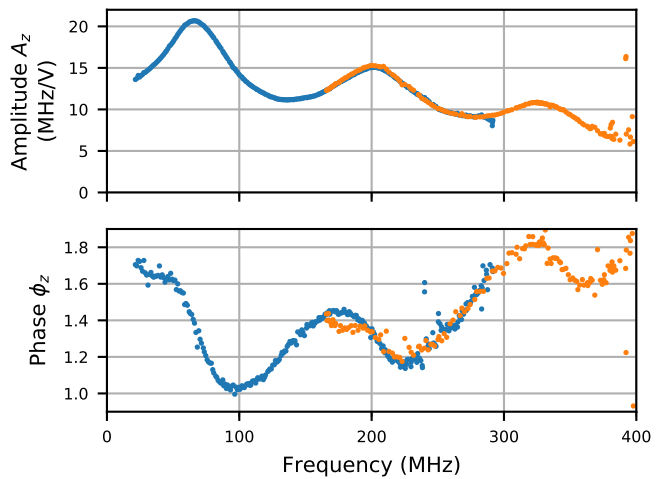


FIG. 3. (a) Amplitude  $A_z$  and (b) phase  $\phi_z$  of the transfer function of the  $z$  control line. Points in blue were measured by varying  $A_x$  at  $\omega_x = \omega_0$  (resonant case), points in orange were measured by varying  $\omega_x - \omega_0$  with fixed  $A_x$  (off-resonant case). The linear component of  $\phi_z(\omega)$ , corresponding to an 8.25ns offset between the transversal and longitudinal drives, was subtracted for clarity.

example, the data for  $\Omega_R = 100$  MHz was taken assuming  $\delta\omega = 0$  but shows (see Fig. 1a) small oscillations for  $\langle\sigma'_x(t)\rangle$  component. This spontaneous detuning can be absorbed in  $\delta\omega$  and does not affect the results of the line calibration.

In addition, we also observed a spurious component  $\Theta_y \neq 0$  due to phase difference between the tomography pulses and the qubit driving pulse. In particular, for  $\delta\omega \neq 0$  the frequency of the driving pulse is different from the resonant tomography pulses which may lead to some phase difference depending on a particular technical details of the pulse generation. This effect can be canceled in the post-processing of the data in Step 3.

*Step 2:* Apply  $x$ -drive as in Step 1, add simultaneous  $z$ -drive at frequency  $\omega_z = |\vec{\Theta}|$ . Use a square pulse envelope for the  $z$  driving pulses and sweep the duration of the  $x$  and  $z$  pulses. Use tomography to reconstruct the evolution of a state vector  $\vec{v}_0(t) = (\langle\sigma'_x(t)\rangle, \langle\sigma'_y(t)\rangle, \langle\sigma'_z(t)\rangle)$ . Due to  $x$ -drive the  $y$  and  $z$  components of the state vector oscillate with the Rabi frequency  $\Omega_R$  while the  $z$ -drive modulates these oscillations at  $\omega_R \ll \Omega_R$  (see Fig. 1b). The duration of the pulses should be long enough to observe these slower oscillations.

*Step 3:* Post-process the data to reconstruct the state vector rotation in the second rotating frame. That step has the benefit of removing the fast Rabi oscillations, thus allowing to take fewer measurements, and allows to fit simpler expressions with less parameters to the data.

To post-process the data we first correct for the phase shift between the  $x$  driving pulse and tomography pulses by applying the transformation  $\vec{v}_1(t) =$

$\exp(\phi_x L_x) \vec{v}_0(t)$ , where  $\phi_x = \arctan(\Theta_y/\Theta_x)$ . To account for the transformation from (2) to (3) we rotate the basis  $\vec{v}_2(t) = \exp(\phi_d L_y) \vec{v}_1(t)$ , where  $\phi_d = -\arctan[\Theta_z/(\Theta_x^2 + \Theta_y^2)^{1/2}]$ . Finally we remove the fast oscillations by going to the second rotating frame  $\vec{v}_3(t) = \exp(i\vec{\Theta} L_x t) \vec{v}_2(t)$ .

The resulting Rabi oscillations of the state vector in the second rotating frame described by  $\vec{v}_3(t) = (\langle \sigma''_x(t) \rangle, \langle \sigma''_y(t) \rangle, \langle \sigma''_z(t) \rangle)$  (see Fig. 1c) are fit to  $\exp(i\vec{\theta}_R \cdot \vec{L}) \vec{v}(0)$ , where both  $\vec{\theta} = (\theta_x, \theta_y, \theta_z)$  and  $\vec{v}(0)$  are fit parameters. The amplitude of the  $z$ -drive can be found as  $A_z = |\vec{\theta}| |\vec{\Theta}| / (\Theta_x^2 + \Theta_y^2)^{1/2}$  and the phase of the drive is given by  $\phi_z = \arctan(\theta_y/\theta_x)$ . Step 3 completes the characterization of the  $z$ -line at the frequency  $\omega_z = \Omega_R$  and the procedure can be repeated for another frequency  $\Omega_R$  controlled by the appropriate choice of  $A_x$  and  $\omega_x$ .

The sensitivity of our method to the phase of  $z$ -drive is demonstrated in Fig. 2. As expected a change in phase of the  $z$ -driving is reliably detected by our procedure. This should be contrasted to the conventional Rabi oscillations as only the amplitude of the drive can be accessed from the frequency of the oscillations while the phase is not accessible.

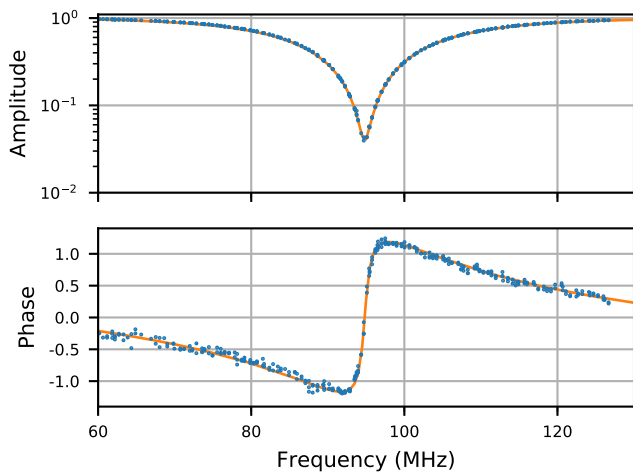


FIG. 4. (a) Amplitude and (b) phase of transmission through a transmission line with a shorted stub resonator. Points in blue were measured with the qubit by comparing  $A_z$  and  $\phi_z$  with and without the stub in place, the orange line was measured directly with a commercial vector network analyzer.

With our method we characterized the complex transfer function in the range of 8 to 400 MHz with an accuracy of 1% for the amplitude and 0.1 rad for the phase. Each point was taken with 4,096 averages at a repetition rate of 40 kHz. The accuracy can be further improved by acquiring more statistics. The measurements at lower frequencies were limited by the decoherence of the qubit with  $T_1 \simeq 2 \mu\text{s}$  and  $T_2 \simeq 2.8 \mu\text{s}$ . However, we point out that the low frequency part of the transfer function can

be also measured with other methods with lower time resolution [1, 3] while *situ* characterization at higher frequencies is currently an unresolved problem. The Rabi oscillations started to deviate from expected simple oscillatory behavior at frequencies  $\simeq 300$  MHz, most probably, due to the excitation of higher levels and technical limitations. More specifically, the pulses applied to the  $x$  line were generated by single-sideband modulation using a quadrature IF (IQ) mixer (Marki/IQ-4509LXP) driven by a local oscillator (LO) and modulated by an arbitrary waveform generator (AWG), to guarantee a fixed phase between the excitation and tomography pulses. The maximum detuning of the driving pulses was ultimately limited by both the mixer and AWG frequency ranges. As our measurement covers the frequency band of the AWG (Tektronix AWG5014C) which can be potentially used to generate  $z$  control pulses we did not investigate this issue further.

As we do not have any other way to measure the transfer function we benchmarked our method by introducing an additional element in the flux line at the room temperature. We used a shorted stub resonator made from a BNC T-adaptor and several meters of a BNC cable shorted at the end. We repeated the characterization for the line with the element and used the original data for the line to de-embed the transfer function of the element itself. The result is shown in Fig. 4 in comparison with the transfer function of the element measured separately with the commercial vector network analyzer (VNA). The agreement between our method and VNA is excellent showing the dynamic range of our method for measuring amplitude of  $\simeq 30$  dB. The dynamic range of a single measurement is bounded by the condition  $\omega_R \ll \Omega_R$  required for the rotating wave approximation in (4) and the decoherence time of the qubit. It can be further improved by dynamically changing the amplitude of the  $z$  drive, taking advantage of the dynamic range of the AWG.

Our method is the first direct *in situ* measurement of the line transfer function from room temperature electronics to a qubit on a chip. The method is most relevant for superconducting qubits whose frequencies are routinely tuned but is applicable for all qubits with  $z$  and  $x$  control. For superconducting qubits one can use our procedure directly to improve the fidelity of the two-qubit quantum gates [8–11] as well as photon-qubit operations requiring non-adiabatic control [1, 4]. In addition to quantum control applications the qubit can be also used as a microscopic probe of the electro-magnetic fields in frequency domain.

We thank Steffen Schlör for help with the experiment. MJ, AF were supported by the Australian Research Council Centre of Excellence CE110001013. AF was supported by the ARC Future Fellowship FT140100338.

---

\* a.fedorov@uq.edu.au

- [1] M. Hofheinz, H. Wang, M. Ansmann, R. C. Bialczak, E. Lucero, M. Neeley, A. D. O'Connell, D. Sank, J. Wenner, J. M. Martinis, and A. N. Cleland, *Nature* **459**, 546 (2009).
- [2] J. Bylander, M. S. Rudner, A. V. Shytov, S. O. Valenzuela, D. M. Berns, K. K. Berggren, L. S. Levitov, and W. D. Oliver, *Phys. Rev. B* **80**, 220506 (2009).
- [3] B. Johnson, *Controlling Photons in Superconducting Electrical Circuits*, Ph.D. thesis, Yale (2011).
- [4] D. Bozyigit, C. Lang, L. Steffen, J. M. Fink, C. Eichler, M. Baur, R. Bianchetti, P. J. Leek, S. Filipp, M. P. da Silva, A. Blais, and A. Wallraff, *Nat. Phys.* **7**, 154 (2011).
- [5] M. Baur, *Realizing quantum gates and algorithms with three superconducting qubits*, Ph.D. thesis, ETH Zurich (2012).
- [6] S. Gustavsson, O. Zwiernik, J. Bylander, F. Yan, F. Yoshihara, Y. Nakamura, T. P. Orlando, and W. D. Oliver, *Phys. Rev. Lett.* **110**, 040502 (2013).
- [7] L. Steffen, Y. Salathe, M. Oppliger, P. Kurpiers, M. Baur, C. Lang, C. Eichler, G. Puebla-Hellmann, A. Fedorov, and A. Wallraff, *Nature* **500**, 319 (2013).
- [8] F. W. Strauch, P. R. Johnson, A. J. Dragt, C. J. Lobb, J. R. Anderson, and F. C. Wellstood, *Phys. Rev. Lett.* **91**, 167005 (2003).
- [9] L. DiCarlo, J. M. Chow, J. M. Gambetta, L. S. Bishop, B. R. Johnson, D. I. Schuster, J. Majer, A. Blais, L. Frunzio, S. M. Girvin, and R. J. Schoelkopf, *Nature* **460**, 240 (2009).
- [10] R. C. Bialczak, M. Ansmann, M. Hofheinz, E. Lucero, M. Neeley, A. D. O'Connell, D. Sank, H. Wang, J. Wenner, M. Steffen, A. N. Cleland, and J. M. Martinis, *Nat Phys* **6**, 409 (2010).
- [11] T. Yamamoto, M. Neeley, E. Lucero, R. C. Bialczak, J. Kelly, M. Lenander, M. Mariantoni, A. D. O'Connell, D. Sank, H. Wang, M. Weides, J. Wenner, Y. Yin, A. N. Cleland, and J. M. Martinis, *Phys. Rev. B* **82**, 184515 (2010).